Structural, electrical and photocatalytic properties of iron-containing soda-lime aluminosilicate glass and glass-ceramics

Ahmed S. Ali[a,b†], Irfan Khan[a†], Bofan Zhang[a], Marta Razum[c], Luka Pavić[c], Ana Santić[c], Paul A Bingham[d], Kiyoshi Nomura[a], Shiro Kubuki[a]

[a]*Department of Chemistry, Graduate School of Science and Engineering, Tokyo Metropolitan University, 1-1 Minami-Osawa, Hachi-Oji, Tokyo 192-0397, Japan*

[b] *Department of Physics, Faculty of Science, Al-Azhar University, Assiut, 71542, Egypt*

[c]*Division of Materials Chemistry, RuđerBošković Institute, Bijeničkacesta 54, 10000 Zagreb, Croatia*

[d] *Materials and Engineering Research Institute, Faculty of Science, Technology and Arts, Sheffield Hallam University, Howard Street, Sheffield S1 1WB, UK*

[†]Corresponding Author (I.K.)
Phone: +81-702-798-0926
E-mail: khan-irfan@ed.tmu.ac.jp

Keywords Soda-lime alumino-silicate glass-ceramics, Iron oxide, Mössbauer spectroscopy, Impedance spectroscopy, Photo-Fenton, Combustible waste slag

Abstract

The structure and electrical conductivity of iron-containing soda-lime alumino-silicate glass-ceramic system were investigated and used for the degradation of methylene blue (MB) solution. Mössbauer isomer shifts were decreased from 0.26 and 0.25 to 0.14 and 0.12 mm s^{-1} with increasing basicity from 0.75 to 1.50 revealing the cleavage in network structure due to the incorporation of Ca^{2+} ions. By increasing basicity from 0.75 to 1.50, the electrical conductivity was increased from (2.2×10^{-12} to 2.2×10^{-8} Ω^{-1} cm^{-1}). More increase in basicity to 1.75 decreased the conductivity to 6.5×10^{-9} Ω^{-1} cm^{-1}. The electrical conductivity is ionic in nature and was correlated to the microstructure of the samples. The first-order rate constant (*k*) for the MB degradation was enhanced from 0.09×10^{-1} to 1.15×10^{-1} min^{-1} with increasing basicity from 0.75 to 1.50, having a good correlation with microstructure and electrical conductivity.

1. Introduction

The dyestuff ismostly responsible for the release of large quantities of highly coloredpollutants and the textile industry corresponding to more than 15% of the total world production of dyes [1-3]. Among organic dyes produced, anionic and cationic dyes represent about 50%–70% of the total market in global production [4]. Dyes effluent contains a high value of TOC (2900mgL^{-1}), BOD (>80mgL^{-1}), and COD (>150mgL^{-1})[5].Molten slag produced during the iron-making and steel-making processes has been a major environmental issue for many years. Up to now, recycling and utilization of these slags allowed recycling of blast furnace slag into Portland blast-

furnace slag cement material, roadbed material, and concrete aggregate. However, steelmaking slag has not been intensively utilized owing to its high basicity [6]. The municipal waste slag discharged from incineration plantsis also used as raw materials of cement and aggregates in concretes[7].However, the development of novel and more effective recycling techniques and technologies is considered highly important for the future based on sustainable energy.

The structure of slag has a similar composition to the widely used commercial glasses wherealumino-silicates are not only among the dominant constituents of the Earth's crust but also of widespread application in the glass and ceramics industries. The effects of iron oxide, which is also the most abundant transition metal in the Earth's crust, on the structure of silicate glasses and melts have been investigated because of its geological and industrial importance [8]. Iron can be added to silicate glasses to improveproperties such as chemical durability and ultraviolet absorption [9, 10].Although the abundance of iron varies in different natural silicates; it remains present in amounts that can influence their properties.Theproperties of natural silicate melt are strongly influenced by iron content since iron occurs in two valence states (Fe^{2+} and Fe^{3+}) with different oxygen coordination [8].Compared to TiO_2, iron oxides have lower bandgap energy so it can be used as heterogeneous catalysts since it has good oxidation-reduction potential and can generate hydroxyl radicals after the addition of an oxidizing agent (e.g., H_2O_2).Since slag contains iron oxides incorporated in silicate glass,it can be regarded aspractical material to use as a photocatalyst for the degradation of organic dyes combining high-value recycling method of slag and low-cost

photocatalyst. However,more study of the parameters affecting its photocatalytic properties, which are mainly controlled by its composition, is needed.

There are no many papers concerning the effect of Fe_2O_3 and basicity on the structure of complexglass-ceramics systemsregarding its application as photocatalyst. Most of the literature focuses on properties related to the metallurgical application. For example, Kang et al [6] studied the thermal conductivity of the molten CaO-SiO_2-FeO*x*system. They reported that the thermal conductivity is significantly decreased as the content of FeO*x* increases, particularly at lower basicity.Chuang et al [11] studied the effects of basicity (CaO/SiO_2) and FeOcontent on the softening and melting temperatures of the CaO-SiO_2-MgO-Al_2O_3 slag system.Rehackovaet al [12]investigated the temperature dependence of the viscosity of the molten CaO-Al_2O_3-SiO_2 system and the impact of CaO/SiO_2 ratio on viscosity and structure of this system. Wu et al [13] reported that for CaO-MgO-SiO_2-Al_2O_3-Cr_2O_3-Fe_2O_3 slag systems with different basicity and different Fe_2O_3 contents, the basicity of the slag changed the mineralogical phases, while the variation of Fe_2O_3 content in slag with the same basicity did not affect the main crystalline phases.On the other hand, some published papers reported the use of silicate glasses and glass-ceramics in the field of dyes degradation. Kubuki et al [14], studied the relationship between local structure and visible light-activated catalytic effect of iron-containing soda lime silicate glass with the composition of $15Na_2O$-15CaO-xFe_2O_3·(70-x)SiO_2, x = 5–50 wt%. The results showed that the first-order rate constant of MB decomposition (k) was estimated to be 2.87×10^{-2} h^{-1} due to the precipitated hematite after heat-treatment of glass samples at 800°C for 100 min.Iida et al[15] reported that iron alumino-silicate glass, $15Na_2O$-15CaO·$40Fe_2O_3$-$11Al_2O_3$-

19SiO_2 (wt%), which has a similar composition to CWS, showed a photocatalytic effect after heat treatment at 1000°C for 100min, with a *k* (pseudo-first-order rate constant)of $9.26 \times 10^{-3}min^{-1}$ for MB degradation. Khan et al [16] also prepared iron-containing aluminosilicate glass by a sol-gel method, which provided a *k* value of 8.61×10^{-2} min^{-1} in the photo-Fenton degradation of MB, where the amount of precipitated hematite was increased by the introduction of Al_2O_3.

In the field of using slag as photocatalyst for organic dyes degradation, some efforts were done,particularly related to the presence of active oxides in these slags. Nasuha et al [1] investigated slag as an effective Fenton catalyst for the photodegradation of methylene blue (MB) and acid blue 29 (AB29). The highest degradation efficiency can reach up to 94% for MB under optimal conditions of $1gL^{-1}$ of catalyst, 20 mM H_2O_2, and pH 3. They[17] also studied the use of iron slag derived from an electric arc furnace (EAFS) as a catalyst to degrade Reactive Black 5 (RB5) after subjected to 0.1M NaOH solution treatment and thermal treatment denoted as A-EAFS. Under optimal conditions of 0.2g L^{-1} A-EAFS, 8mM H_2O_2, and pH 3.0, A-EAFS sustained nearly 94% RB5 removal. Ishikawa et al [18] reported that heat treatment of waste slag recycled glass-ceramics (WSRG) with additional Fe_2O_3 content of 10, 30 and 50 mass% decomposed MB aqueous solution with first-order rate constants (*k*) of 2.6, 2.3 and 2.7×10^{-3} min^{-1}, respectively, under visible light irradiation. The degradation was related to the precipitated amount of α-Fe_2O_3 nanoparticles.In our previous work[19], we succeeded in preparing glass and glass-ceramics from municipal waste slag by melt-quenching, obtaining *k* values of up to 2.2×10^{-2} min^{-1} by melting the slag at 1400 °C, then

subsequently heat treating it at 800 °C for 100 min while it was 2.8×10^{-2} min^{-1} for the sample prepared using chemical reagents by excluding the impurities.

The investigation and understanding of the electrical conductivity of the glass arevery important. Generally, silicate glasses are poor conductors of electricity at least at room temperature. The electrical conductivity of alkali silicate glasses essentially depends on the concentration of the charge carriersand their mobility [20].Alkali ions are the most mobile species in the non-crystalline alkali silicate materials where self-diffusion of alkali ions generally occurs as an exchange of cationic pairs between sites. If enough energy is applied to an ion, such as an applied electric field, or thermal fluctuations, the atom can more easily jump between sites [21]. Nishida et al[22] reported that glass prepared using fly ash shows an electrical conductivity from 10^{-8} to 10^{-6} S cm^{-1} due to electron hopping from less distorted $Fe^{II}O_6$octahedra to distorted $Fe^{III}O_4$tetrahedra. Khater et al[23] studied the effect of CaO/SiO_2 (0.2–0.93 mol %) on the electrical properties of some glass materials. The samples with relatively low CaO/SiO_2 molar ratios have higher electrical conductivity, compared to the other samples with higher CaO/SiO_2 molar ratios. Dutta et al[24] studied the conductivity of alkali ions in soda-lime-silicate glasses (Na_2O-CaO-SiO_2) at a frequency range from 50 Hz to 1 MHz and temperature range from room temperature to 603 K. The silica content was fixed while the Na_2O was increased on the expense of CaO. They found that the conductivity increased by increasing the Na_2O content from 20 to 25due to the increase in the mobile ions. Natrup et al[25] studied the mobilities of calcium and sodium ions in silicate glasses of compositions $x$$Na_2O$-(3- x) CaO-4SiO_2 with x = 0.0, 0.1, 0.3, 1.0 and 3.0. They measured the activation energy of Ca^{2+} diffusionin the pure calcium silicate

glass and it was higher than the activation energy of the electrical conductivity. They concluded that the electrical conductivity of this glass is not determined by the migration of Ca^{2+} ions, but by impurity charge carriers, which are most likely Na^{+} ionsintroduced by $CaCO_3$ used in the preparation.

This work aims to investigate the influence of Fe_2O_3 and basicity (CaO/SiO_2) on the structure, electrical and photocatalytic properties of iron-containing soda lime-aluminosilicateglass-ceramics.This can improve our knowledge about controlling the condition required for higher dyes degradation using these slag systems.

2. Experimental

2.1. Materials

Analytic grade ingredients of (SiO_2: Kanto Kagaku 37974-00), ($CaCO_3$: Wako 03000385), (Al_2O_3: Wako 012-01965), (Fe_2O_3: Wako 096-04825) and (Na_2CO_3: Wako 199-01585), ($H_2O_2$30%: Wako 081-04215) and methylene blue (MB: $C_{16}H_{18}N_3SCl_3 \cdot H_2O$, Wako 133-06962). The slag used in this study was collected in July 2018 at the Tamagawa municipal waste combustion plant (Ohta-Ku, Tokyo, Japan)according to the agreement between Tamagawa municipal waste combustion plant and faculty of science - Tokyo metropolitan university.

2.2. Sample preparation

The glass-ceramic samples were prepared in two steps. In the first step, the glass samples were prepared by the melt quenching method and in the second step, glasses were subjected to a controlled heat-treatment to obtain glass-ceramics. In the melt-quenching process, the melt was heated at 1400°C for 1h in a platinum crucible andsamples were obtained by quenching the base of the crucible in ice-cold water.Glasses were then thermally treated at 800 °C for 100 min. To investigate the influence of Fe_2O_3 and basicity (CaO/SiO_2) on the structure and photocatalytic properties of iron-containing soda lime-aluminosilicate glass-ceramics, samples were prepared according to the system $5Na_2O$-$20Al_2O_3$-xFe_2O_3-((75-x)/2)CaO-((75-x)/2)SiO_2.The CaO/SiO_2 ratios are fixed to 1, while the content of Fe_2O_3 was varied to 3, 6, 12 and 18%.According to the iron oxide content, the samples are denoted F-3, F-6, F-12 and F-18. After getting the photocatalytic results, the sample F-6 was chosen as a model systemfor its best properties, and another series of samples were prepared by keeping fix amount of the Fe_2O_3 at6% while CaO/SiO_2 was varied from 0.75 to 1.00, 1.25, 1.50 and 1.75 where the samples were denoted as B-0.75, B-1.00, B-1.25, B-1.50 and B-1.75, respectively.For the modified slag, one gram of as collected slag was mixed with amounts of chemicals(Na_2O; 0.106, Al_2O_3; 0.403, SiO_2; 0.604; CaO; 1.02 gram) to decrease the iron content to 6% and increase the basicity to 1.50, all were mixed in an electric agate mortar for 30 min to ensure its homogeneity then melted at 1400 °C for 1h in a platinum crucible. The modified sample denoted as M-1.50 was obtained by quenching the base of the crucible in ice-cold water followed by theheat-treatment at

800 °C for 100 min. The XRF compositional analysis of the as collected slagand the nominal composition of model slagis presented in Table 2.

2.3. Characterization techniques

The structureof heat-treated samples was characterized by ^{57}Fe Mössbauer spectroscopy, X-ray diffractometry (XRD) Transmission electron microscopy (TEM) and Impedance spectroscopy (IS). ^{57}Fe Mössbauer spectra were measured using a constant acceleration spectrometer. A source of 925MBq^{57}Co (Rh) was attached to an MVT-1000 transducer connected to an MDU-1200 drive unit. The drive unit was connected to a DFG-1200 digital function generator with 1200 channels. Transmitted γ-rays were detected by a proportional counter. The signals were amplified by an ORTEC 142 preamplifier. The applied voltage (2 kV) was obtained by using an ORTEC 556 High voltage–power supply, and an ORTEC 570 amplifier. The amplified signals were monitored with a PC via an ORTEC EASYMSC. Samples with weight = 40 mg were homogeneously dispersed in a circular sample holder with 10 mm diameter; inserted into the spectrometer, and measured until the total counts collected were greater than 10^6. Isomer shifts are given relative to α-Fe, which was measured as a reference. The Mösswinn 3.0i XP software was used to analyze the obtained spectra. XRD patterns were recorded using a RINT TTR3, Rigaku diffractometer between 2θ of 10° to 80°, with precision and scan rates of 0.02 and 5°/ min, respectively. Cu-Kα X-rays (λ = 0.1541nm) were generated at 50kV and 300mA, and monochromated. TEM images were obtained using a JEM-3200FS Field Emission Energy Filter Electron Microscope.

Electrical properties were studied by Impedance spectroscopy (IS).Complex impedance was measured using an impedance analyzer (Novocontrol Alpha-N Dielectric Spectrometer, Novocontrol) at room temperature in a wide frequency range from 0.04 Hz to 1 MHz. The samples were prepared in the form of pellets (5 mm in diameter and ~0.75 mm thick).Gold electrodes, 3.8 mm in diameter, were sputtered onto both sides of sample pellets as contacts using Sputter coater SC7620, Quorum Technologies. Experimental data were analyzed by equivalent circuit modeling using the complex nonlinear least-square (CNLLSQ) fitting procedure and the corresponding parameters were determined. This procedure is based on the fitting of experimental impedance to an appropriate equivalent circuit model.The values of the resistance obtained from the fitting procedures, R, and electrode dimensions (d is sample thickness and A is electrode area) were used to calculate the DC conductivity, $\sigma_{DC} = d/(R \times A)$.

3. Results and discussion

3.1. Structural characterization

3.1.1.XRD

XRD patterns of the prepared samples are shown in Fig. 1. By changing the Fe_2O_3 content from 3 to 18 (wt%) at fixed basicity (CaO/SiO_2),Fig. 1 (a), it can be seen that the sample's crystallinity and peaks intensity increase. The detected phases for F-3 are Nepheline ($NaAlSiO_4$: PDF No. 00-019-1176), calcium aluminum oxide ($Ca_3Al_2O_6$: PDF No. 00-032-0148) and sodium peroxide (NaO_2: PDF No. 01-089-5950). For F-6, only Nepheline (PDF No. 00-035-0424) and calcium iron oxide ($CaFeO_3$: PDF No. 01-

071-6763) can be detected. The gehlenite phase ($Al_2Ca_2SiO_7$: PDF No. 01-089-5917) can be detected for the samples F-12 and F-18 along with nepheline and calcium iron oxide.

XRD patterns of the samples with different basicity and fixed $Fe_2O_3$are presented in Fig. 1 (b). The sample with lower basicity B-0.75 showsan almost amorphous structure. By increasing the basicity, crystallinity and peaks intensity increase. The sample B-1.25 shows peaks that can be assigned as gehlenite and calcium iron oxidewhile B-1.50 shows peaks related to gehlenite (PDF No. 01-077-1113) and larnite(Ca_2SiO_4: PDF No. 01-076-3609). More increase in basicity to 1.75 resulted in peaks of gehlenite and Ca_2SiO_4. This matches that the change in basicity can change the detected phases [13].To apply the results obtained for this system to the practical slag, XRD patterns for the as collected slag, melted slag and modified one are shown in Fig. 1 (c). The as collected slag whichhas Fe_2O_3content of 18.33 wt% and its basicity is 1.00 (see Table 2) shows amorphous structure while after melting at 1400 °C for 1h and heat-treatment at 800 °C for 100 min, it shows some peaks related to calcium silicate (Ca_2SiO_4: PDF No. 00-024-0234) and iron silicate oxide ($Fe_{2.95}SiO_{0.05}O_4$: PDF No. 00-052-1140). The modified slag M-1.50shows peaks due to gehlenite (PDF No. 01-074-1607) and calcium iron oxide ($Ca_2FeO_{3.5}$: PDF No. 00-038-0508). It can be noticed that for all samples with basicity higher than 1.00, the gehlenite phase, which is considered as a good supporting material for photocatalyst [26], can be detected which maybe considered as an advantage for these samples.

3.1.2.Mössbauer spectroscopy

^{57}Fe Mössbauer spectra and the fitted parameters for all samples measured at room temperature are presented in Fig. 2 and Table 1. The samples with different $Fe_2O_3$and fixed basicity,Fig. 2 (a), show two doublets related to tetrahedral $Fe^{III}$with isomer shifts range (0.15–0.32 mm s^{-1}). The lowest iron oxide content sample of 3wt% has too noisy spectra so it is not presented. No magnetic sextet for hematite or any other iron oxide can be detected. By increasing Fe_2O_3, the isomer shifts were found to increase from 0.23, 0.21 mm s^{-1} for F-6 to 0.28, 0.24 and 0.32, 0.26 mm s^{-1} for F-12 and F-18, respectively. The samples with controlled basicity, Fig. 2 (b), show also two doublets related to tetrahedral Fe^{III}. By increasing the basicity from 0.75 to 1.50, the isomer shifts are decreased from0.25 and 0.26 mm s^{-1} to 0.12 and 0.14 mm s^{-1}.Further increase in basicity to 1.75 increasedthe isomer shift to 0.12 and 0.19 mm s^{-1} which is almost the same for sample B-1.25.

As collected slag shows two doublets with δ = 0.48 and 1.01 mm s^{-1} related to $Fe^{III}O_h$ and $Fe^{II}O_h$, respectively. The absorption areas for Fe^{II} and Fe^{III} are 70.2 and 29.8 %, respectively, this means that the amount of $Fe^{II}$is much larger than of Fe^{III}which is similar to our previous paper[19]where the absorption areas for Fe^{II} and Fe^{III}were 85.5 and 14.5 %, respectively. After melting, slag shows doublets related to Fe^{III}only with δ = 0.35 and 0.36 mm s^{-1}. The change in oxidation state fromFe^{II} to $Fe^{III}$is expected since a higher melting temperature of 1400 °C compared to 1200 °C in the incineration plant and more oxygen availabilityfavoursthe oxidation of Fe^{II} ions. The modified slag M-1.50 has two doublets both related to $Fe^{III}T_d$ with δ = 0.18 and 0.26 mm s^{-1}, respectively.Althoughthese values are higher than that for the model slag system B-1.50

(δ = 0.12 and 0.14 mm s^{-1}),they are still in the range of$Fe^{III}T_d$ and much less than those of the melted slag.

3.1.3. TEM

The TEM images of the controlled basicity samples are presented in Fig. 3. No crystalline phases can be detectedfor the sample B-0.75. By increasing the basicity, particles can be detectedwith a typical size of 12, 23 and 58 nm for the samples B-1.00, B-1.25 and B-1.50, respectively.Further increase in basicity to 1.75 resulted in a decrease in particle size to 25 nm.

3.2. Electrical measurements

Fig. 4 (a) shows the conductivity spectra for samples of the basicity from 0.75 to 1.75 (B-0.75-B-1.75). For samples with basicity $\geq$ 1.25 conductivity isotherms are similar in shape and different spectral features can be observed. A nearly frequency-independent conductivityrelated to the long-range transport of charge carriers which corresponds to DC conductivity can be observed at low frequencies, whereas with increasing frequency conductivity dispersion occurs with an increase in a power-law fashion which is related to their localized short-range motions. Also, in the lowest-frequency region of spectra for B-1.50 and B-1.75 samples, a decrease in conductivity is visible. This behavior is associated with the electrode polarization effect due to the accumulation of mobile ions (i.e. Na^+ and Ca^{2+}) at the blocking metallic electrode and is

typical for ion-conducting glasses and glass-ceramics. On the other hand, for samples withbasicity of 0.75 and 1.00, in our experimental frequency window, the DC conductivity plateau is not attained and the conductivity is strongly frequency-dependent.

As a step forward,we analysed the complex impedance plots by equivalent circuit modeling using the complex nonlinear least-square (CNLLSQ) fitting procedure, see Fig.5. One can see that spectra for samples B-0.75 and B-1.00 arenot well-defined, while for other samples spectrum shows a similar shape consisting of two semicircles and a low-frequency spur. The corresponding equivalent circuit models used for fitting of the experimental data are shown in Fig. 5 and determined fitting parameters are listed in Table SM-1.According to the appropriate equivalent circuit model used, various processes can be identified and separated based on the order of magnitude of obtained fitting parameters(capacitance/resistance)[27, 28]. The proposed interpretation refers to ceramics, but it can be used for other similar solid materials such as glass-ceramics. The complex impedance spectra of samples B-1.00 to B-1.75 are described by two parallel equivalent circuits (R-CPE) connected in series. For the low-frequency spur which appeared in the impedance spectra for these samples(except for B-1.00),the third CPE element connected inseries is added to the model.The semicircle at higher frequencies corresponds to the sample bulk(equivalent circuit R1-CPE1), whereas the semicircle at low frequencies (R2-CPE2), is probably associatedwith thegrain boundaries from the multiple crystalline phases or/andminor crystalline phase(s) in obtained partially crystallized samples.It should be noted that as the basicity is decreasing, the spur is also

decreasing and finallydisappears for sample B-1.00 together with low-frequency semicircle (sample B-0.75) from the impedance spectra.

From the values of resistance, obtained from equivalent circuit modelingalong with sample geometry,we evaluated thetotal DC conductivity for all B-series samples, see Table 3. The values of DC conductivity correspond to the range ~10^{-12} – 10^{-8} $(\Omega\ cm)^{-1}$. The variation of DC conductivity as a function of CaO/SiO_2 ratio is presented in Fig. 4 (b).The lowest conductivity value was observed forB-0.75 sample, $\sigma_{DC} = 2.2\times10^{-12}(\Omega\ cm)^{-1}$.With increasing the CaO/SiO_2 ratio up to 1.50, the amount of CaO is increasing up to 43.9 wt%,with a fixed amount of Fe_2O_3 at 6 wt%, leading to the increase in the DC conductivity for four orders of magnitude reaching the highest value of 2.2×10^{-8} $(\Omega\ cm)^{-1}$. These results suggest that the DC conductivity is highly dependent on the composition and microstructure as the spatial arrangements of the building network with available interstices are changed making it easy for ions to migrate. It should be mentioned that the Mössbauer structure analysis refers to isomer shifts related only to Fe^{3+} for all samples with controlled basicity. Therefore, it can be inferred that the conductivity is ionic in nature and there is no additional polaronic contribution to the total conductivity due to electron hopping of Fe^{3+}-Fe^{2+}, characteristic for mixed valance transition metal oxides. The electrical conductivity is directly proportional to the number of charge carriers and their mobility [29]. In our case,these parameters are being affected through the introduction of CaOwhich increases the concentration of Ca^{2+} ions andcreates more non-bridging oxygens (NBO) which facilitates the movement of both types of charge carriers, Ca^{2+} and Na^{+} ions.

However, the decrease in DC conductivity is observed for B-1.75 sample. By adding more CaO, Ca^{2+} ions can be incorporated in the interstitial positions together with the Na^{+} ions [28], which result intheir decreased mobilityin a disordered silicate network and consequently have an impact on the overall conductivity. Moreover, additional factors which could contribute to the observed conductivity should not be excluded. The conductivity may be affected by the crystalline phases where the samples with basicity $\geq$ 1.25 show the gehlenite phase however, the intensity of the peaks of gehlenite decreased for B-1.75 compared to B-1.50. Also, it should be noted that the DC conductivity trend correlates with the change in the microstructure where it is obvious from TEM measurements that the particle size increases by increasing basicity up to B-1.50 while it decreases for B-1.75.

Schwartz and Mackenzie[30] measured the electrical resistivity of xCaO·(1–x)4SiO_2 glasses with x varying between 0.4 and 0.55. The resistivity decreased with the calcium oxide content x and they attributed the conductivity to the migration of Ca^{2+} ions. Malki et al[31] found that the activation energies for the dc conductivities are in the range from 1.38 to 1.51 eV, and they also ascribed the electrical conductivity to the diffusion of Ca^{2+} ions.On the other hand, Natrup et al[25]studied the mobilities of calcium and sodium ions in silicate glasses of compositions $x$$Na_2O$·(3–$x$)CaO· 4$SiO_2$ with x= 0.0, 0.1, 0.3, 1.0 and 3.0. In the pure calcium silicate glass (x=0), the activation energy of Ca^{2+} diffusion is higher than the activation energy of the electrical conductivity. They concluded that the electrical conductivity of this glass is not determined by the migration of Ca^{2+} ions, but by impurity charge carriers, which are most likely Na^{+} ions present in the $CaCO_3$ used in the preparation.

Considering that in our prepared glass-ceramics Na_2O, Fe_2O_3 and Al_2O_3 content is fixed while CaO is increased at the expense of SiO_2, the conductivity trend can be explained based on both, changes of the concentration of mobile ions and structural disorder of these samples. Increasing basicity will increase the concentration of Ca^{2+} ions, however, the conductionpaths for Ca^{2+} as well as Na^{+} ions are affected by the microstructure in partially crystallized glass samples.

In the glass-ceramics in which the grain boundary blocks the transport of mobile ions, the decrease in the size of the crystalline grains increases the volumetric contribution of the grain/particle boundaries, hence lowering the conductivity [32]. In our system, increasing basicity from 0.75 to 1.50 increased the average size of the crystalline grains from 12 to 58 nm which could lead to the conduction pathways which are less destroyed and obstructed. On the other hand, increasing basicity to 1.75 resulted in a decrease in the particle size to 25 nm which hindered the ionic transport, hence decreasing the conductivity even though the sample contains more mobile ions.

The modified slag sample M-1.50 has a DC conductivity of $5.6\times10^{-9}\,\Omega^{-1}\,cm^{-1}$ which is less than the conductivity of the sample B-1.50 although both samples have the same Fe_2O_3 content and basicity. This can be attributed to the impurities in the slagsuch as TiO_2, MgO, P_2O_5, K_2O and MnO (see Table 2) which affect the structure of the glass-ceramic and, consequently, the motion of the conductive ions in this sample. In particular, it should be noted that both B-1.50 and M-1.50 samples contain ghelenite as a major phase. However, while B-1.50 contains Ca_2SiO_4as a minor phase, in M-1.50 sample a small amount of $Ca_2FeO_{3.5}$ is detected, See Fig. 1.

3.3. Photocatalytic measurements

3.3.1. Effect of $Fe_2O_3$and basicity

The kinetic dye degradation measurements of methylene blue for the samples with different Fe_2O_3content at fixed basicityunder photo Fenton are presented in Fig. 6. The results show that by increasing the iron oxide content from 3 to 6wt%, the *k* value increased from 0.41 to 0.66 × 10^{-1} min^{-1}. More increase in Fe_2O_3 resulted in a decrease in *k* value to 0.59 and 0.29 × 10^{-1} min^{-1} for the samples F-12 and F-18, respectively. While the increase in iron oxide can promote degradation,further increase leads to a decrease in MB degradation as it acts as a scavenger and reacts with·OH radicals [1].The Mössbauer isomer shift of F-6 is the lowest which matches our previous work [19] where the lowest iron oxide content having the lowest isomer shifts promotes the photo-Fenton reaction. The blank sample (only MB+H_2O_2) and the dark samples (without irradiation) have very low *k* values of (0.06, 0.05, 0.07, 0.07 and 0.04 × 10^{-1} min^{-1}) for the blank, F-3, F-6, F-12 and F-18, respectively.

The sample F-6 is the best performing sample, therefore it has been chosen for studying the effect of basicity in the range 0.75 to 1.75. The Kinetic dye degradation measurements of methylene blue for these samples are presented in Fig. 7. It can be seen that there is a direct relationship between the *k* value and basicity. The estimated *k* values were 0.09, 0.66, 0.80 and 1.15 × 10^{-1} min^{-1} for the samples B-0.75, B-1.00, B-1.25 and B-1.50, respectively. Further increase in basicity to 1.75 causes the *k* value to decrease to 0.72 × 10^{-1} min^{-1}. It can be noticed also that the effect of basicity on the MB degradation is significantly higher than the effect of iron oxide content. The dark

samples (without irradiation) have *k* values of (0.02, 0.07, 0.07, 0.08 and 0.07 × 10^{-1} min^{-1}) for B-0.75, B-1.00, B-1.25, B-1.50 and B-1.75, respectively. Looking at the XRD, it is clear that the intensity of the peaks gets higher and sharper with increasing basicity up to B-1.50 which has the most intense peaks. For B1.25, B-1.50 and B-1.75 the main peak is assigned to gehlenite which is considered as a good supporting material [26] while in the case of B-1.00, the main peaks were related to nepheline and calcium iron oxide. By increasing basicityto B-1.75, the intensity of the main peak assigned asgehlenite decreased while the peaks of the other phase,Ca_2SiO_4were increased which may explain the decrease in *k* value.

Also by considering the relation between the Mössbauer isomer shifts,*k* values and basicityFig. 8, we can see thatisomer shifts decreased with basicity revealing the distortion in the structure due to introducing CaO which can further help in the movement of the hydroxyl radicals. This trend is reversed for sample B-1.75where an increase in the isomer shifts to (0.12 and 0.19 mm s^{-1}), almost the same for sample B-1.25, can be noticed which may explain the comparable *k* value for both samples.The contribution of the particle size of the samplesshould be considered as it reflects the microstructure effect. The particle size increases as basicity increases (Fig. 3) up to B-1.50 then decreasing for B-1.75. By increasing the particle size, the hopping of charge carriers was facilitatedwhich resulted in higher conductivity [33, 34]. Amano et al [35] investigated the effect of the particle size on the photocatalytic activity of tungsten trioxide (WO_3) for water oxidation. The photocatalytic activity for water oxidation increased with increasing particle size because the surface recombination of

photogenerated electrons and holes occurred less frequently where the fast recombination mostly occurred on the surface.

In our case where ionic conductivity is the prominent one, the effect of particle size on the conductivity and hence on the photoactivity should be taken into consideration. As discussed before, *k* values increase along with the conductivityand particle size up to B-1.50 then all decreased for B-1.75.

3.3.2. Proposed mechanism

The key component in our catalyst is Fe_2O_3. However, as Fe_2O_3 photocatalyst has a nano-size diameter, it is necessary to have an appropriate matrix to support it. Glass and glass-ceramics are good candidates as supporting materials since it is widely diffused, low-cost, resistant to high temperatures, adsorbent, non-toxic material and can enhance the photocatalyst performance. This can be achieved by enhancing recyclability which is necessary for practical applications. The efficiency of glass-ceramics supported photocatalyst depends on tailoring catalyst compositions, in our case, by controlling Fe_2O_3 content and basicity. The results show that the degradation is correlated to the system structure and Fe_2O_3 oxidation state. Both have been investigated using XRD, TEM and Mössbauer. Based on the results of MB degradation, the proposed mechanism can be discussed as follows:

In dark conditions, classical Fenton, which is initiated by Fe^{2+}, is excluded since iron oxide is present as Fe^{3+} as confirmed by Mössbauer measurements. Also, Fenton reaction requires low and narrow working pH (typically 2-4) while in our case pH is ≥

7. Direct reduction of Fe^{3+} on the catalyst surface by H_2O_2 can occurs according to the reaction.

$$Fe^{3+}/Fe_2O_3 + H_2O_2 \rightarrow Fe^{2+}/Fe_2O_3 + HO_2^{\bullet} + H^+ \quad (1)$$

However, the degradation in dark is very small (almost 10% of the degradation in light conditions) due to low mobility and high recombination rate consequently, this reaction can be excluded. On the other hand, in light conditions, possible reactions may contribute to MB degradation. Firstly, photoreaction where H_2O_2 can dissociate to hydroxyl radicals;

$$H_2O_2 + h\nu \rightarrow 2\,HO^{\bullet} \quad (2)$$

However, the degradation in blank sample is much less and light wavelength required for this reaction should be$\leq$ 360 nm (in our case, λ is 420-750 nm). Secondly, direct light excitation of Fe_2O_3 without H_2O_2 is negligible due to its high recombination rate and low mobility.

$$Fe_2O_3 + h\nu \rightarrow Fe_2O_3\,(e^- + h^+) \quad (3)$$

$$h^+ + H_2O \rightarrow HO^{\bullet} + H^+ \quad (4)$$

Thirdly, heterogeneous photo-Fenton reaction which is the most prominent reaction for MB degradation under visible light condition using soda lime aluminosilicate glasses and H_2O_2. Irradiation of Fe_2O_3 using visible light can generate electron-hole pair on the surface of the catalyst converting Fe^{3+} to Fe^{2+} which in turn reacts with H_2O_2 producing hydroxyl radicals. Hydroxyl radicals attack the dyes leaving degradation products.

$$Fe^{3+}/Fe_2O_3 + h\nu \rightarrow Fe^{3+}/Fe_2O_3\,(e^- + h^+) \quad (5)$$

$$Fe^{3+}/Fe_2O_3 + e_{CB} \rightarrow Fe^{2+}/Fe_2O_3 \quad (6)$$

$$Fe^{2+}/Fe_2O_3 + H_2O_2 \rightarrow Fe^{3+}/Fe_2O_3 + HO^{\bullet} + OH \quad (7)$$

The morphology contributes in degradation mechanism as well. The particle size increases with increasing basicity up to 1.50. In this case, the surface recombination of photo-generated electrons and holes occurs less frequently because fast recombination mostly occurs on the surface. Also, as the particle size increases, the blocking of mobile charges transport by grain boundaries is reduced giving more chance for these charges to immigrate to the surface of the catalyst to initiate photo-Fenton reaction. The proposed mechanism is consistent with the results of Mössbauer, TEM, electrical and photocatalytic measurements.

3.3.3.The modified slag

The obtained results were applied to modify the practical slag to the same composition of the best performing sample B-1.5 and denoted as M-1.50. This can provide a low-cost photocatalyst under visible light and photo-Fenton. After the composition of the slag was modified by addingamounts of chemicals to decrease the iron content to 6wt% and increase the basicity to 1.50, it was prepared under the same melt quenching method. Figure 7 shows that M-1.50 has a *k* value of 1.14×10^{-1} min^{-1} which is almost the same for the model sample. The XRD pattern,Mössbauer spectra and parameters of the modified sample are presented in Fig.1 (c), Fig. 2 (c) and Table 1, respectively.Although the isomer shifts (0.26 and 0.18 mm s^{-1}) is higher than B-1.50 isomer shifts(0.14 and 0.12),this difference didn’t affect its performance mostly due to

that it contains gehlenite as the main phase similarly asB-1.50. The *k* values for as collectedslag and melted slag (0.15 and 0.22 × 10^{-1} min^{-1}) are much less than that of modified slag M-1.50(1.14 × 10^{-1} min^{-1}) which indicates the efficiency of the suggested modified system. The enhancement in the degradation can beattributed to the higher electrical conductivity for the modified slag (5.6×10^{-9} Ω^{-1} cm^{-1}). Also, the existence of TiO_2 (2.14%) and MgO (3.12%) can promote degradation.

IR spectra for the modified sample M-1.50 and model sample B-1.50 is presented in Fig. 9. As can be seen, both spectra havethe same main peaks which further confirm the successful modification of slag. The peaks at 480, 520 and 720 $cm^{-1}$are due to Si–O–Si and O–Si–Ovibrations [36] while the peak at 850 cm^{-1} is attributed Al–O bonds stretching vibration of AlO_4tetrahedra. The peaks at 910 and 990 cm^{-1} can be attributed to the asymmetrical stretching vibration of O–Si–O bonds in SiO_4 tetrahedrons [12]. The peaks around 1640 and 3460 cm^{-1} relates to OH bending vibration modes [37, 38].

3.3.4. Parameters affecting the degradation

The study of different parameters affecting the degradation is presented in Fig. 10 and Fig. 11. In the photo-Fenton reaction, the most important parameters are the H_2O_2 concentration and pH. As it can be seen for the H_2O_2 concentration Fig. 10 (a) the degradation is only 50% in the H_2O_2concentration of 10 mM. Increasing the concentration to 0.1 and 0.2 M increases the degradation to 79.7 and 83.7% after 60 min, respectively, while the highest degradation of 96.9 % can be achieved for H_2O_2 of 0.35 M after 30 min. This is because more active radicals can be produced [39].

However, excess H_2O_2(0.8 M) decreases the degradation to 84.3% after 60 min, mostly because it acts as a scavenger of hydroxyl radicals [39, 40]. The best-performing H_2O_2 concentration was found to be 0.35 M, which produced a *k* value of 1.15×10^{-1} min^{-1}.

The effect of pH is illustrated in Fig. 10 (b) the best performance was at 11 pH with the degradation of 95.3% after 15 min, however, the sample shows good degradation ability over a wide range of pH with longer times which means that the prepared catalyst can overcome the narrow range of pH in the case of the classical Fenton reaction. In our case, MB, which is a cationic dye,is adsorbed more quickly at higher pH and consequently, an increase in the MB degradation rate is expected [41, 42]. It was reported that in acidic solutions, the surfaces of photocatalysts are positively charged while they are negatively charged in alkaline solutions [43]. As a result, the efficiency of MB photodegradation is expected to increase with pH, owing to electrostatic interactions between the negative surface of the catalyst and the MB cations. The effect of MB concentration is clear in our case. Fig.10 (c)shows that almost the same degradation value around 95% can be achieved for MB concentration of 20, 40 and 60 μM, however, the time required in the case of 40 and 60 μM is almost four times longer than that of 20 μM. This can be attributed to the decrease in ·OH radical generation due to the coverage of catalyst active sites by the adsorbed dye [41].The catalyst dosage effect was also studied with a catalyst loading of 2, 4 and 8 g/L and the results are shown in Fig.10 (d). Increasing the catalyst dosage from 2 to 4 g/L the degradation increased from 87.5 to 96.9% mostly due to the increase in the active surfaces for the same unit volume of MB [1], which leads to an increase in the absorbed photons and generation of OH radicals. More catalyst 8 g/L lead to a decrease in degradation to

93.8% which can be caused by a reduction in light intensity as the solution opacity increases [44] or that at higher catalyst loading, the iron act as a scavenger and reacts with OH radicals [1]. The change in the efficiency based on catalyst loading is not remarkable which can be an advantage for using the lowest amount as it has almost the same degradation ability.

Fig.11, shows the influence of the reaction temperature on MB removal. It can be seen that with increasing temperature, the rate of the reaction was 0.10, 1.13, 1.29 and 1.58×10^{-1} min^{-1} at 298K, 303K, 308K, and 313K, respectively. The activation energy (E_a), estimated using the rate constants (k_t) from the Arrhenius equation [39], was calculated according to Eq. (1)

$$\ln k_t = -E_a/RT + \ln A \qquad (1)$$

Where k_t is the reaction rate constant as a function of temperature; E_a ($J \cdot mol^{-1}$) is the apparent activation energy; R is the universal gas constant of 8.314 $J \cdot mol^{-1} \cdot L^{-1}$; T (K) is the absolute temperature; A is the Arrhenius pre-exponential factor.

The apparent activation energy of MB obtained in this study Fig. 11 was 24.89kJ mol^{-1}which is much less than the E_a reported by Nasuha et al(56.68 kJ mol^{-1})in the case of the degradation of Reactive Black 5 using activated electric arc furnace slag as a heterogeneous Fenton-like catalyst [17].This result indicatesthe higher efficiencyof our samples.

3.3.5. Reusability

In this study, the reusability of the best-performing samples B-1.5 and modified slagM-1.50 with catalyst loading (4 g/L) was tested for the degradation of MB (20 μM) at room temperature, initial pH of 10 and H_2O_2 of 0.35 M. Fig. 12 illustrates the MB degradation efficiency tested at 30 min of irradiation after 5 successive cycles where the degradation was decreased by 10.3and 12.6% for B-1.50 and M-1.50, respectively. The repeated measurements were carried out by centrifuging the solution followed by removing and replacing it with a new MB solution. No further filtration or drying of the powder was carried out between subsequent experiments, which can further lower the operational cost if the catalyst were applied in a large-scale process.

4. Conclusion

Glass-ceramic system with different Fe_2O_3 and CaO/SiO_2 ratio were prepared by the controlled heat-treatment of glasses synthesized by melt-quenching. The structure of the samples was investigated using XRD, Mössbauer spectroscopy and TEM. The CaO/SiO_2 ratio has a much higher effect on the structure and photoactivity compared to the effect of Fe_2O_3. The photocatalytic ability of the prepared samples was influenced by the change in the (micro)structure. An inverse relationship between Mössbauerisomer shifts and *k* values for methylene blue degradation was found for thesamples with basicity in the range 0.75 – 1.75.The direct relationship correlates the MB degradation with the increase in basicity from 0.75 to 1.50. More increase in basicity has a negative effect on degradation. DC conductivity was found to be ionic in nature. The conductivity increased from (2.2×10^{-12} to 2.2×10^{-8} Ω^{-1} cm^{-1}) with

increasing basicity from 0.75 to 1.50 while it decreases to 6.5×10^{-9} Ω^{-1} cm^{-1} for the basicity of 1.75. It was found that photocatalytic ability increases with the crystallinity, particle size and electrical conductivity of the samples. The CWS with modified composition has almost the same *k* value of the model slag. The obtained results are promising for the degradation of wastewater using the modified CWS under visible light and photo-Fenton reaction.

AcknowledgementsThis work was supported by the Tokyo Metropolitan Government Advanced Research Grant Number H29-1.

References

[1] N. Nasuha, S. Ismail, H. Hameed, Activated electric arc furnace slag as an effective and reusable Fenton-like catalyst for the photodegradation of methylene blue and acid blue 29, J. Environ. Manag. 196 (2017) 323–329. https://doi.org/10.1016/j.jenvman.2017.02.070.

[2] A.N. Módenes, F.R. Espinosa-Quinones, D.R. Manenti, F.H. Borba, S.M. Palácio, A.Colombo, Performance evaluation of a photo-Fenton process applied to pollutant removal from textile effluents in a batch system,J. Environ. Manag.104 (2012) 1–8.https://doi.org/10.1016/j.jenvman.2012.03.032.

[3] M. Fayazi, M.A. Taher, D. Afzali, A. Mostafavi, Enhanced Fenton-like degradation of methylene blue by magnetically activated carbon/hydrogen peroxide with

hydroxylamine as Fenton enhancer, J. Mol.Liq. 216 (2016) 781–787.https://doi.org/10.1016/j.molliq.2016.01.093.

[4] I.K. Konstantinou, T. A. Albanis, TiO_2-assisted photocatalytic degradation of azo dyes in aqueous solution: kinetic and mechanistic investigations A review, ApplCatal B-Environ 49 (2004) 1–14.https://doi:10.1016/j.apcatb.2003.11.010.

[5] A. Buthiyappan, A. Abdul Aziz, W.M.A.W. Daud, Recent advances and prospects of catalytic advanced oxidation process in treating textile effluents, Rev. Chem. Eng. 32 (2016) 1–47. https://doi. 10.1515/revce-2015-0034.

[6] Y. Kang, K. Nomura, K. Tokumitsu, H. Tobo, K. Morita, Thermal conductivity of the molten CaO-SiO2-FeOx system, Metallurgical and Materials Transactions B, 43 (2012) 1420–1426. https://doi.10.1007/s11663-012-9706-7.

[7] T. Nanba, Y.Kuroda, S. Sakida, Y. Benino, Chemical recycling of municipal waste slag by using phase separation, Ceram. Soc. Japan 117 (2009) 1195–1198.

[8] M. Ahmadzadeh, J. Marcial, J. MCloy, Crystallization of iron-containing sodium aluminosilicate glasses in the $NaAlSiO_4$-$NaFeSiO_4$ join, Res. Solid Earth 122 (2017) 2504–2524.https://doi:10.1002/2016JB013661.

[9] P.A. Bingham, J.M. Parker, T. Searle, J.M. Williams, K. Fyles, Redox and clustering of iron in silicate glasses,Glass Technol.: Eur. J. Glass Sci. Technol. A,253 (1999) 203-209 J. Non-Cryst. Solids. https://doi.org/10.1016/S0022-3093(99)00361-0.

[10] N.J. Cassingham, P.A. Bingham, R.J. Hand, Property modification of a high level nuclear waste borosilicate glass through the addition of Fe_2O_3, Glass Technol.: Eur. J. Glass Sci. Technol. A,49 (2008) 21-26.

[11] H.C. Chuang, W.S. Hwang, S.H. Liu, Effects of Basicity and FeO Content on the Softening and Melting Temperatures of the CaO-SiO_2-MgO-Al_2O_3 Slag System, Materials Transactions, 50 (2009) 1448–1456. https://doi:10.2320/matertrans.MRA2008372.

[12] L. Rehascova, S. Rosypalova, R. Dudek, J. Kukutschova, J. Dobrovska, Effect of CaO/SiO_2 ratio on viscosity and structure of slag, Metalurgija, 54 (2015) 455–458.

[13] X.R. Wu, R.T. Wang, H.H. Lü, X.M. Shen, L.S. Li, Influence of basicity and Fe_2O_3 on crystallisation characteristics of CaO–MgO–SiO_2–Al_2O_3–Cr_2O_3–Fe_2O_3 system, Mater.Res.Innov.19 (2015) 1–6.https://doi:10.1179/1432891715Z.0000000002191.

[14] S. Kubuki, J. Iwanuma, Y. Takahashi, K. Akiyama, Z. Homonnay, K. Sinko, E. Kuzmann, T. Nishida, Visible light activated catalytic effect of iron containing soda-lime silicate glass characterized by 57Fe-Mössbauer spectroscopy, J. Radioanal. Nucl. Chem. 301 (2014) 1–7.https://doi:10.1007/s10967-014-3109-y.

[15] Y. Iida, K. Akiyama, B. Kobzi, K Sinkó, Z. Homonnay, E. Kuzmann, M. Ristić, S. Krehula, T. Nishida, S. Kubuki, Structural analysis and visible light-activated photocatalytic activity of iron-containing soda lime aluminosilicate glass, J. Alloys. Compd. 645 (2015) 1–6.https://doi.org/10.1016/j.jallcom.2015.04.153.

[16] I. Khan, K. Nomura, E. Kuzmann, Z. Homonnay, K. Sinkó, M. Ristić, S. Krehula, S. Musić, S. Kubuki, Photo-Fenton catalytic ability of iron-containing

aluminosilicate glass prepared by sol-gel method, J. Alloys. Comp. 816 (2020) 1–7. https://doi:10.1016/j.jallcom.2019.153227.

[17] N. Nasuha, S. Ismail, H. Hameed, Activated electric arc furnace slag as an efficient and reusable heterogeneous Fenton-like catalyst for the degradation of Reactive Black 5, J. Taiwan Inst. Chem. E. 67 (2016) 235–243.https://doi.org/10.1016/j.jtice.2016.07.023.

[18] S. Ishikawa, B. Kobzi, K. Sunakawa, S. Nemeth, A. Lengyel, E. Kuzmann, Z. Homonnay, T. Nishida, S. Kubuki, Visible-light activated photocatalytic effect of glass and glass ceramic prepared by recycling waste slag with hematite, Pure Appl. Chem. 89 (2017) 535–554. https://doi:10.1515/pac-2016-1018.

[19] A.S. Ali, K. Nomura, Z. Homonnay, E. Kuzmann, A. Scrimshire, P.A. Bingham, S. Krehula, M. Ristić, S. Musić, S. Kubuki, The relationship between local structure and photo- Fenton catalytic ability of glasses and glass- ceramics prepared from Japanese slag, J. Radioanal. Nuc. Chem. 322 (2019) 751–761.https://doi.org/10.1007/s10967-019-06726-z.

[20]M.L. Braunger, C.A. Escanhoela Jr., I. Fier, L. Walmsley, E.C. Ziemath, Electrical conductivity of silicate glasses with tetravalent cations substituting Si, J. Non-Cryst. Solids 358 (2012) 2855–2861. https://doi:10.1016/j.jnoncrysol.2012.07.013.

[21]R.S. Welch, C.J. Wilkinson, J. C. Mauro, C.B. Bragatto, Charge Carrier Mobility of Alkali Silicate Glasses Calculated by Molecular Dynamics, Front. Mater. 6(2019) 1–6.https://doi.org/10.3389/fmats.2019.00121.

[22] T. Nishida, M. Tokunaga, Y. Sugata, S. Kubuki, Mssbauer study of semiconducting and ferrimagnetic fly ash-recycled glass, J. Radioanal. Nucl. Chem. 266 (2005) 171–177.

[23] G.A.Khater, M.M. Gomaa, J. Kang,M.A. Mahmoud, Effect of CaO/SiO_2 molar ratio on the electrical and physical properties of basaltic glass materials,Heliyon 5 (2019) 1–17.https://doi.org/10.1016/j.heliyon.2019.e01248.

[24] A. Dutta, T.P. Sinha, P. Jena, S. Adak, Ac conductivity and dielectric relaxation in ionically conducting soda–lime–silicate glasses, J. Non-Cryst. Solids 354 (2008) 3952–3957. https://doi:10.1016/j.jnoncrysol.2008.05.028.

[25] F.V. Natrup, H. Bracht, S. Murugavel, B. Roling, Cation diff usion and ionic conductivity in soda-lime silicate glasses, Phys. Chem. Chem. Phys. 7 (2005) 2 2 7 9 – 2 2 8 6. https://doi:10.1039/b502501j.

[26] H. Wu, W. Peng, Z.M. Wang, K. Koike, Cerium-doped gehlenite silver/silver chloride for continuous photocatalysis, RSC Adv. 6 (2016) 37995–38003.https://doi: 10.1039/c6ra02444k.

[27] J.T. Irvine, D.C. Sinclair, A.R. West, Electroceramics: Characterization by Impedance Spectroscopy, Advanced Materials. 2 (1990) 132–138.

[28] D.C. Sinclair, Characterization of Electro-materials using ac Impedance Spectroscopy,Boletín de la Sociedad Española de Cerámica y Vidrio, 34 (1995) 55–65.

[29] F.M. EzzEldin, N.A. El Alaily, Electrical conductivity of some alkali silicate glasses, Mater. Chem. Phys. 52 (1998) 175–179.https://doi.org/10.1016/S0254-0584(98)80021-7.

[30] M. Schwartz, J. D. Mackenzie, Ionic Conductivity in Calcium Silicate Glasses, J. Am. Ceram. Soc., 49 (1966) 582–585.

[31] M. Malki, M. Micoulaut, F. Chaimbault, Y. Vaills, P. Simon, Percolative conductivity in alkaline-earth silicate melts and glasses, 64 (2003) 661–667. https://doi.org/10.1209/epl/i2003-00278-2.

[32] A.M. Cruz, E.B. Ferreira, A.C.M. Rodrigues, Controlled crystallization and ionic conductivity of a nanostructured LiAlGePO4 glass–ceramic, J. Non-Cryst. Solids 355 (2009) 2295–2301.https://doi.org/10.1016/j.jnoncrysol.2009.07.012.

[33] E. Yuliza, R. Murniati, A. Rajak, Khairurrijal, M. Abdullah, Effect of Particle Size on the Electrical Conductivity of Metallic Particles, ICAET conference paper (2014) 151–154.https://doi:10.2991/icaet-14.2014.37.

[34] B.S. Avinash, V.S. Chaturmukha, H.S. Jayanna, C.S. Naveen, M.P. Rajeeva, B.M. Harish, S. Suresh, R.L. Ashok, Effect of Particle Size on Band Gap and DC Electrical Conductivity of TiO_2 Nanomaterial, AIP conference paper (2015) 1–4. http://dx.doi.org/10.1063/1.4946477.

[35] F. Amano, E. Ishinag, A. Yamakat, Effect of Particle Size on the Photocatalytic Activity of WO_3 Particles for Water Oxidation, J. Phys. Chem. 117 (2013) 22584−22590.https://doi:dx.doi.org/10.1021/jp408446u.

[36] M.Y. Hassaan, A.G. Mostafa, H.A. Saudi, M.A. Ahmed, H.M.H. Saad, DC and AC cnductivity study of Basalt glasses containing high concentrations of Na^+ ions, Silicon 10 (2018) 2153–2160.https://doi: 10.1007/s12633-017-9744-5.

[37] M.M. Rashad, A.A. Ibrahim, D.A. Rayan, M.M.S. Sanad, I.M. Helmy, Photo-Fenton-like degradation of Rhodamine B dye from waste water using iron molybdate catalyst under visible light irradiation, Environ. Nanotechnol. Monit. Manag. 8 (2017) 175–186.https://doi.org/10.1016/j.enmm.2017.07.009.

[38] G. Liang, Y. Li, C. Yang, C. Zi, Y. Zhang, X. Hu, W. Zhao, Production of biosilica nanoparticles from biomass power plant fly ash, J. Waste Manag. 105 (2020) 8–17.https://doi.org/10.1016/j.wasman.2020.01.033.

[39] R. Saleh, A. Taufik, Degradation of methylene blue and congo-red dyes using Fenton, photoFenton, sono-Fenton, and sonophoto-Fenton methods in the presence of iron (II,III) oxide/zinc oxide/graphene (Fe_3O_4/ZnO/graphene) composites, Sep. Purif. Technol. 210 (2019) 563–573.https://doi.org/10.1016/j.seppur.2018.08.030.

[40] S. Guo, G. Zhang, J. Wang, Photo-Fenton degradation of rhodamine B using Fe_2O_3–Kaolin as heterogeneous catalyst: Characterization, process optimization and mechanism, J. Colloid Interface Sci. 433 (2014) 1–8. https://doi.org/10.1016/j.jcis.2014.07.017.

[41] K.M. Reza, A.S.W. Kurny, F. Gulshan, Parameters affecting the photocatalytic degradation of dyes using TiO_2: a review, Appl. Water Sci. 7 (2017) 1569–1578. https://doi.10.1007/s13201-015-0367-y.

[42] M.H. Abdellah, S.A. Nosier, A.H. El-shazly, A.A. Mubarak, Photocatalyticdecolorization of methylene blue using TiO_2/UV system enhanced by air sparging, Alex. Eng. J. 57 (2018) 3727–3735.https://doi.org/10.1016/j.aej.2018.07.018.

[43] Z.W. Tang, C.P. Huang, Inhibitory Effect of Thioacetamide on CdS Dissolution During Photocatalytic Oxidation of 2, 4-Dichlorophenol,Chemospher 30 (1995) 1385–1399.

[44] N. Soltani, E. Saion, M.Z. Hussein, M. Erfani, A. Abedini, G. Bahmanrokh, M. Navasery, P. Vaziri, Visible light-induced degradation of methylene blue in the presence of photocatalyticZnS and CdS nanoparticles, Int. J. Mol. Sci., 13 (2012) 12242–12258. https://doi:10.3390/ijms131012242.

Table

Table 1 ^{57}Fe Mössbauer fitted parameters for room temperature analyses of as collected slag (not heat-treated), melted slag at 1400 °C; heat treated at 800 °C for 100 min; and samples with different Fe_2O_3 and basicity content and the modified salag melted at 1400 °C; heat treated at 800 °C for 100 min

Sample	Species	A (%)	δ (mm s^{-1})	Δ (mm s^{-1})	Γ (mm s^{-1})
F-18	Fe^{III} T_d	78.8	$0.32_{\pm 0.01}$	$0.77_{\pm 0.02}$	$0.50_{\pm 0.02}$
	Fe^{III} T_d	21.2	$0.26_{\pm 0.02}$	$1.65_{\pm 0.07}$	$0.45_{\pm 0.05}$
F-12	Fe^{III} T_d	60.0	$0.28_{\pm 0.01}$	$1.00_{\pm 0.03}$	$0.53_{\pm 0.04}$
	Fe^{III} T_d	40.0	$0.24_{\pm 0.01}$	$1.78_{\pm 0.05}$	$0.54_{\pm 0.06}$
F-6 (B-1.00)	Fe^{III} T_d	58.1	$0.21_{\pm 0.02}$	$0.93_{\pm 0.07}$	$0.50_{\pm 0.08}$
	Fe^{III} T_d	41.9	$0.23_{\pm 0.02}$	$1.67_{\pm 0.11}$	$0.53_{\pm 0.11}$
B-1.75	Fe^{III} T_d	50.0	$0.19_{\pm 0.02}$	$0.84_{\pm 0.05}$	$0.39_{\pm 0.07}$
	Fe^{III} T_d	50.0	$0.12_{\pm 0.03}$	$1.73_{\pm 0.09}$	$0.54_{\pm 0.12}$
B-1.50	Fe^{III} T_d	76.4	$0.14_{\pm 0.02}$	$0.92_{\pm 0.04}$	$0.56_{\pm 0.05}$
	Fe^{III} T_d	23.6	$0.12_{\pm 0.03}$	$1.88_{\pm 0.07}$	$0.37_{\pm 0.08}$
B-1.25	Fe^{III} T_d	58.9	$0.20_{\pm 0.01}$	$0.84_{\pm 0.03}$	$0.48_{\pm 0.05}$
	Fe^{III} T_d	41.1	$0.12_{\pm 0.02}$	$1.88_{\pm 0.04}$	$0.44_{\pm 0.06}$
B-0.75	Fe^{III} T_d	60.6	$0.25_{\pm 0.02}$	$0.98_{\pm 0.07}$	$0.51_{\pm 0.05}$
	Fe^{III} T_d	39.4	$0.26_{\pm 0.02}$	$1.61_{\pm 0.13}$	$0.51_{\pm 0.12}$
M-1.5	Fe^{III} T_d	53.8	$0.26_{\pm 0.02}$	$0.82_{\pm 0.06}$	$0.51_{\pm 0.08}$
	Fe^{III} T_d	46.2	$0.18_{\pm 0.02}$	$1.78_{\pm 0.07}$	$0.52_{\pm 0.10}$
Melted slag	Fe^{III} O_h	52.1	$0.36_{\pm 0.01}$	$0.60_{\pm 0.06}$	$0.43_{\pm 0.06}$
	Fe^{III} O_h	47.9	$0.35_{\pm 0.01}$	$1.08_{\pm 0.09}$	$0.51_{\pm 0.06}$
As collected slag	Fe^{II} O_h	70.2	$1.01_{\pm 0.01}$	$1.81_{\pm 0.02}$	$0.47_{\pm 0.03}$
	Fe^{III} O_h	29.8	$0.48_{\pm 0.06}$	$1.32_{\pm 0.09}$	$0.53_{\pm 0.09}$

T_d tetrahedral, O_h octahedral, A absorption area, δ isomer shift, Δ quadrupole splitting, Γ line width

Table 2 XRF compositional analysis of combustible waste slag (weight %) collected July 2018 and nominal composition of the model slag B-1.50

	SiO_2	Al_2O_3	Fe_2O_3	CaO	Na_2O	TiO_2	MgO	P_2O_5	K_2O	MnO	Others
As collected slag	23.90	20.80	18.33	24.61	4.69	2.14	3.12	1.45	0.21	0.36	0.39
B-1.5	27.6	20	6	41.4	5	-	-	-	-	-	-

Table 3 DCconductivity at RT for the samples of basicity 0.75 to 1.75 and the modified slag heat-treated at 800 °C for 100 min

Sample	σ_{DC}[a] / $(\Omega\ cm)^{-1}$
B-0.75	2.2×10^{-12}
B-1.00	3.2×10^{-11}
B-1.25	7.0×10^{-10}
B-1.50	2.2×10^{-8}
B-1.75	6.5×10^{-9}
M-1.50	5.6×10^{-9}

[a] DC conductivity obtained from equivalent circuit modeling.

Figure captions

Fig. 1 XRD patterns of samples (a) effect of Fe_2O_3 heat-treated at 800 °C for 100 min, (b) effect of basicity heat-treated at 800 °C for 100 min and (c) as collected slag (not heat-treated), melted slag and modified slag heat-treated at 800 °C for 100 min

Fig. 2 RT Mössbauer spectra of samples (a) effect of Fe_2O_3 heat-treated at 800 °C for 100 min, (b) effect of basicity heat-treated at 800 °C for 100 min and (c) as collected slag (not heat-treated), melted slag and modified slag heat-treated at 800 °C for 100 min

Fig. 3 Images TEM of the samples of effect of basicity heat-treated at 800 °C for 100 min

Fig. 4 (a) The conductivity spectra for samples of the basicity effect, (b) the relation between the CaO/SiO_2 and DC conductivity

Fig. 5 Complex impedance plots and equivalent circuit modeling for samples of the basicity effect

Fig. 6 Kinetic dye degradation measurements of methylene blue for the samples of effect of Fe_2O_3 heat-treated at 800 °C for 100 min

Fig. 7 Kinetic dye degradation measurements of methylene blue for the samples of effect of basicity heat-treated at 800 °C for 100 min

Fig. 8 The relation between CaO/SiO_2, Mössbauer isomer shifts and *k* values for the samples of effect of basicity heat-treated at 800 °C for 100 min

Fig. 9 IR spectra of the sample B-1.50 and the modified slag M-1.50

Fig. 10 Effect of (a) H_2O_2 concentration, (b) initial pH, (c) Dye concentration and (d) catalyst loading on the methylene blue degradation under visible light for the sample B-1.50 heat-treated at 800 °C for 100 min

Fig. 11 Effect of temperature on the methylene blue degradation under visible light for the sample B-1.50 heat-treated at 800 °C for 100 min

Fig. 12 Reusability of the sample B-1.50 heat-treated at 800 °C for 100 min at room temperature under visible light, pH of 10, catalyst loading 4 g L^{-1}, MB concentration 20 μM and H_2O_2 of 0.35 M

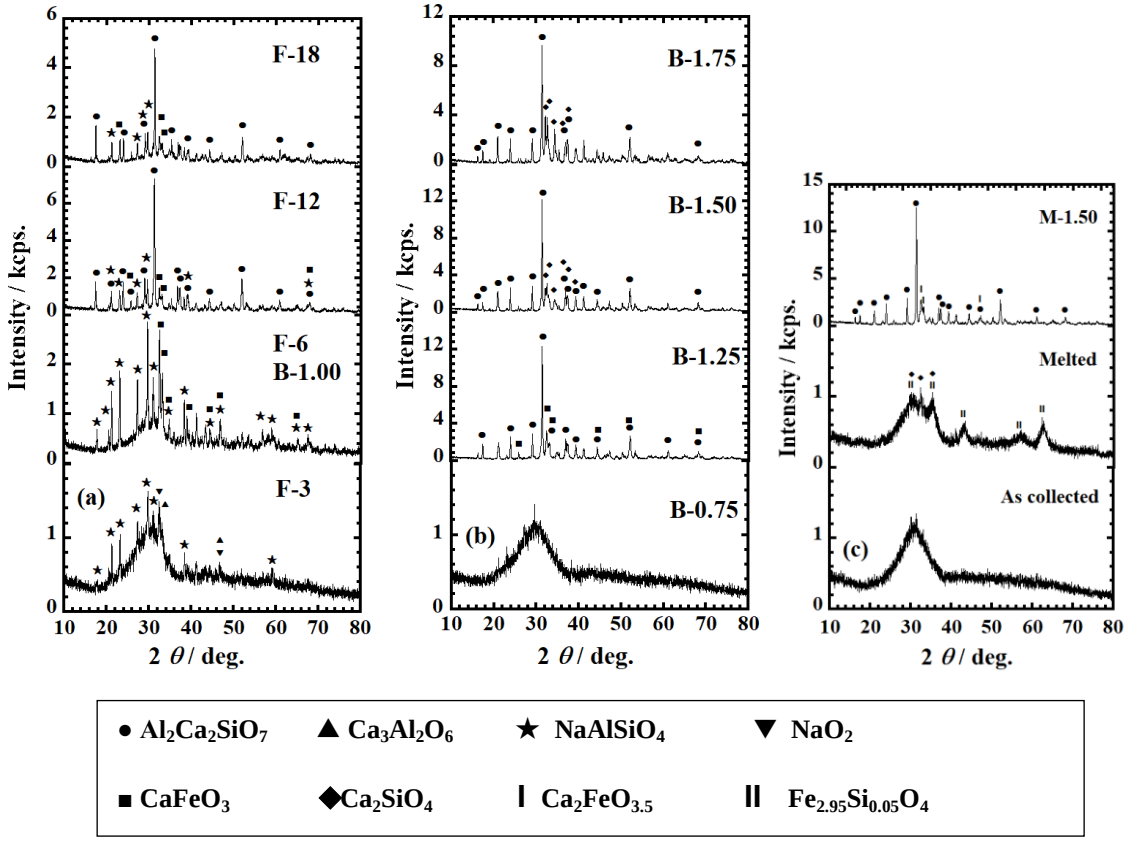

A. S. Ali *et al.*, Fig. 1

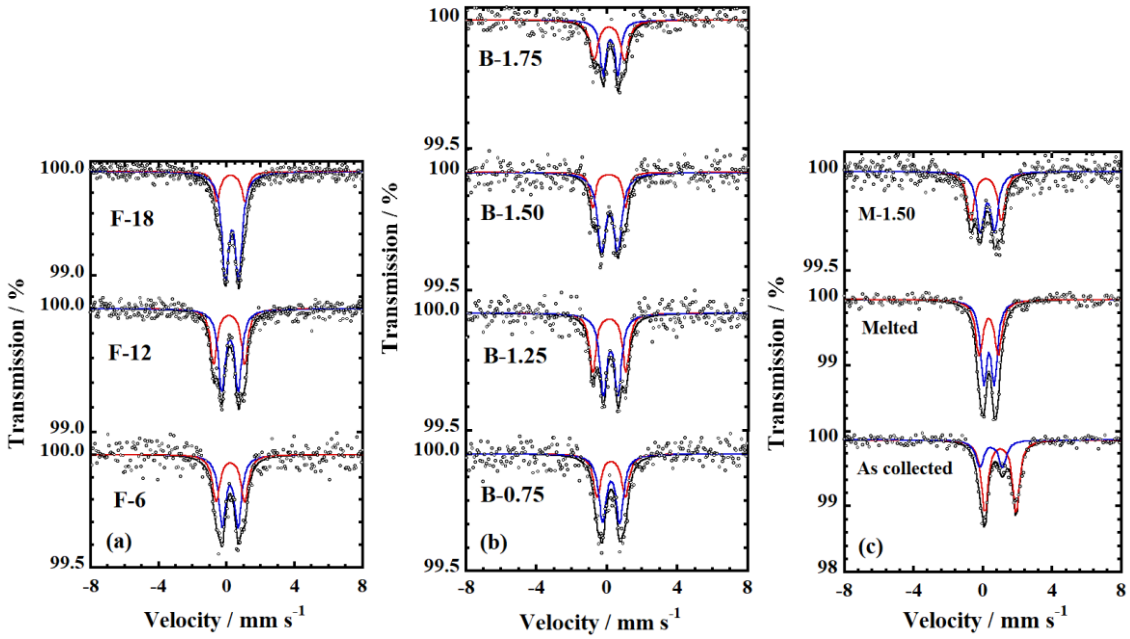

A. S. Ali *et al.*, Fig. 2

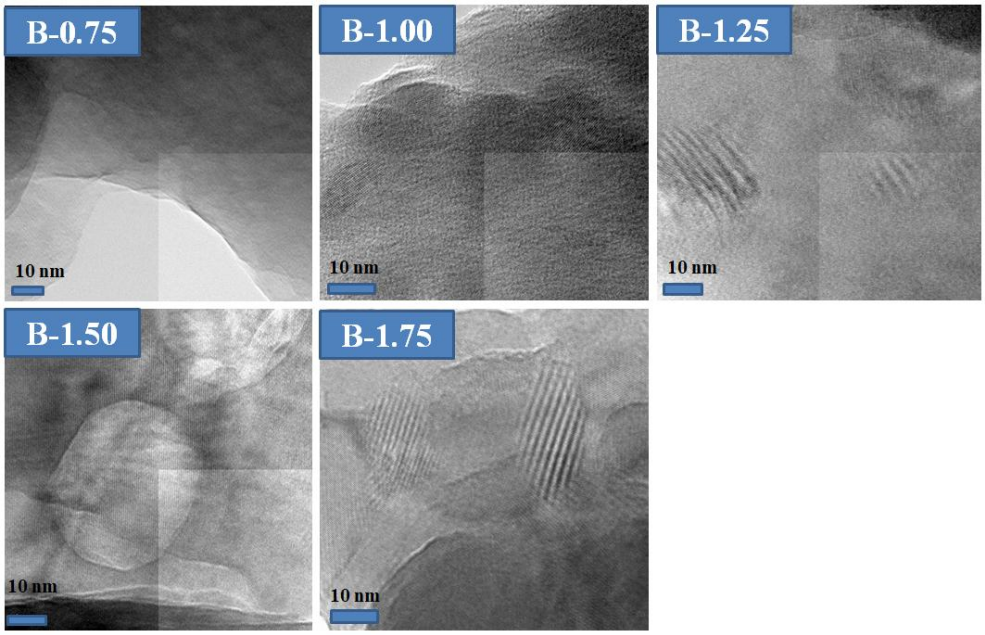

A. S. Ali *et al.*, Fig. 3

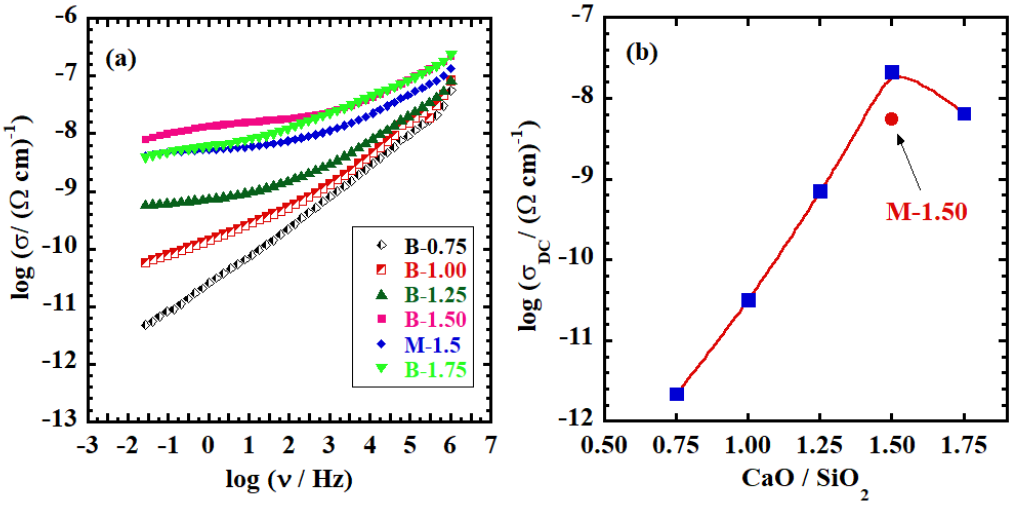

A. S. Ali *et al.*, Fig. 4

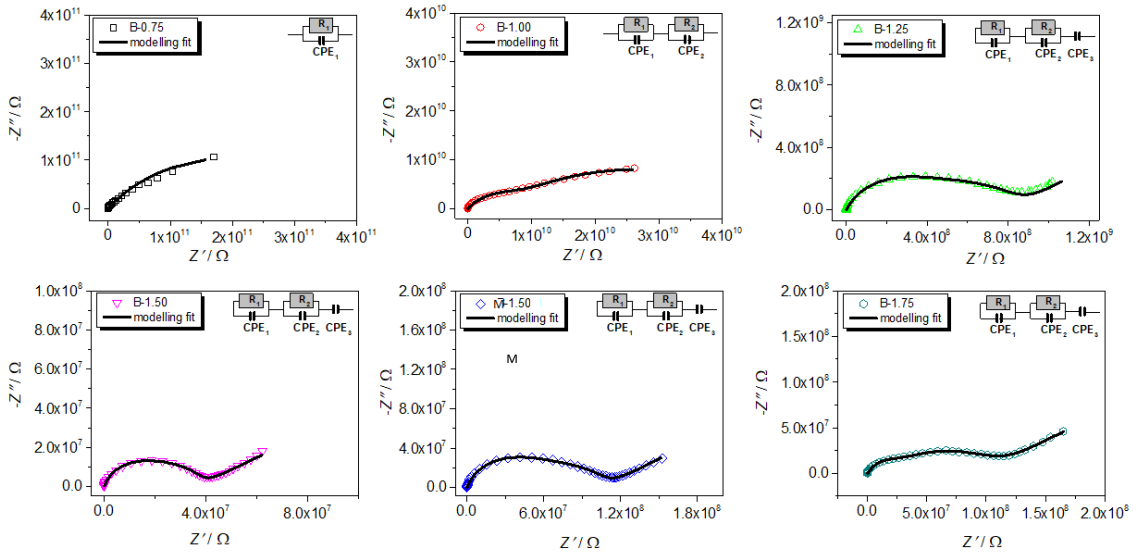

A. S. Ali *et al.*, Fig. 5

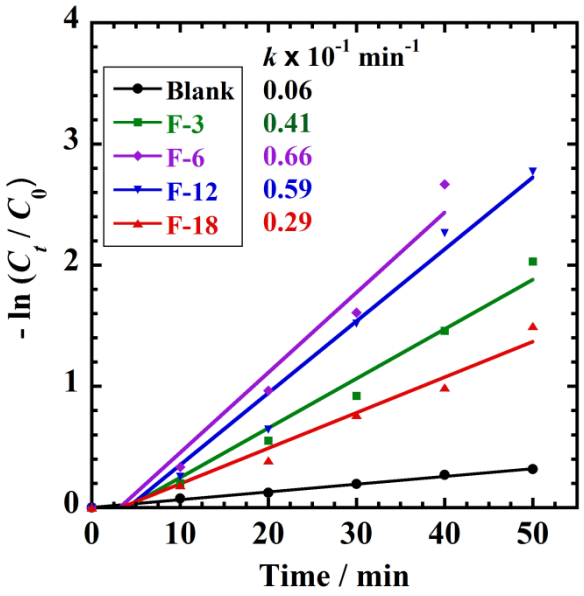

A. S. Ali *et al.*, Fig. 6

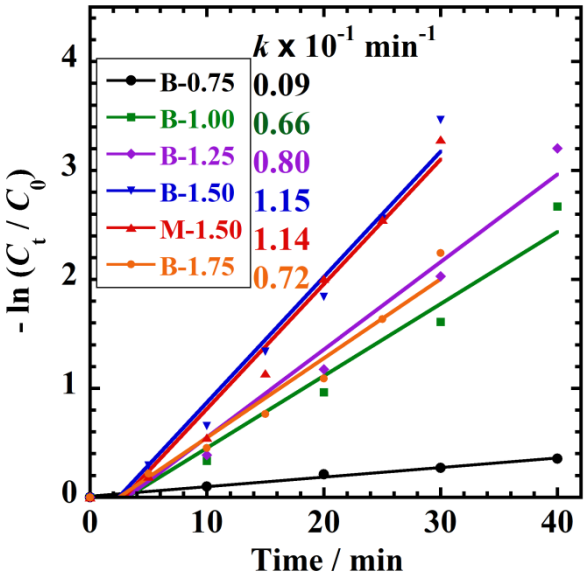

A. S. Ali *et al.*, Fig. 7

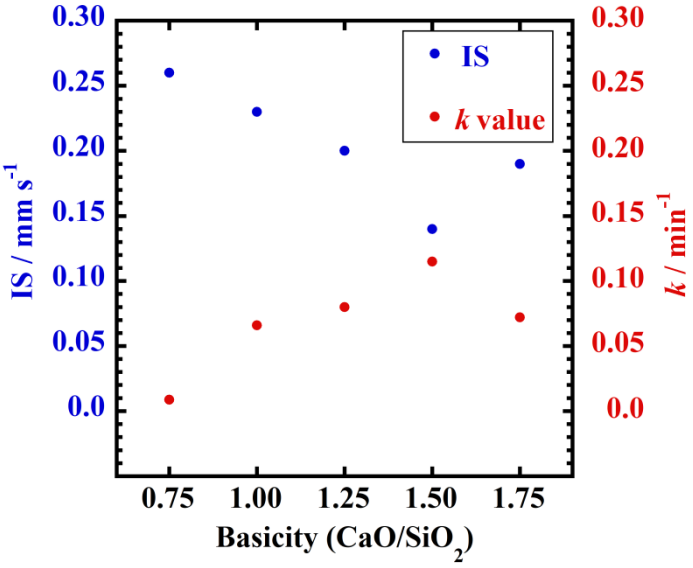

A. S. Ali *et al.*, Fig. 8

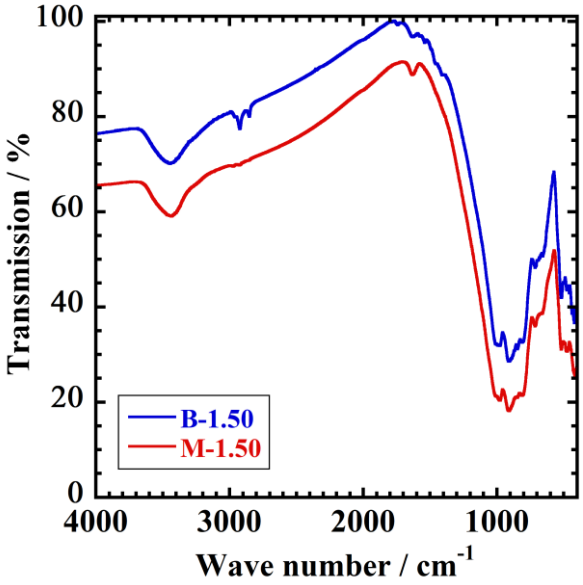

A. S. Ali *et al.*, Fig. 9

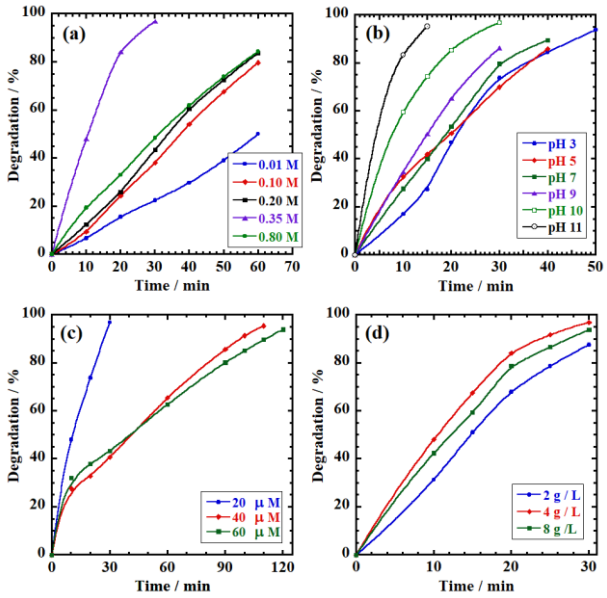

A. S. Ali *et al.*, Fig. 10

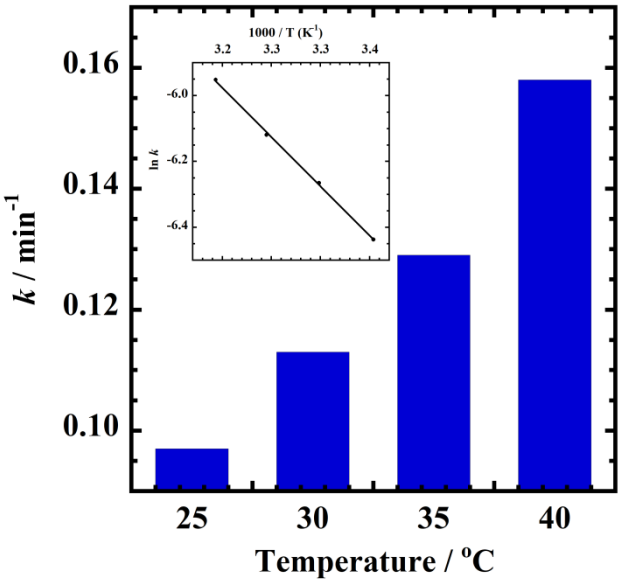

A. S. Ali *et al.*, Fig. 11

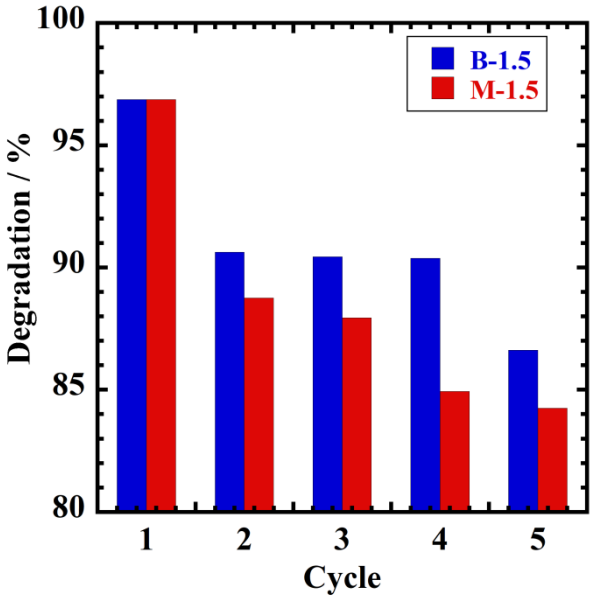

A. S. Ali *et al.*, Fig. 12